

Coalescence of Rotating Black Holes on Eguchi-Hanson Space

Ken Matsuno^{*}, Hideki Ishihara[†], Masashi Kimura[‡] and Shinya Tomizawa[§]

*Department of Mathematics and Physics,
Graduate School of Science, Osaka City University,
3-3-138 Sugimoto, Sumiyoshi-ku, Osaka 558-8585, Japan*

(Dated: November 28, 2018)

Abstract

We obtain new charged rotating multi-black hole solutions on the Eguchi-Hanson space in the five-dimensional Einstein-Maxwell system with a Chern-Simons term and a positive cosmological constant. In the two-black holes case, these solutions describe the coalescence of two rotating black holes with the spatial topologies of S^3 into a single rotating black hole with the spatial topology of the lens space S^3/\mathbb{Z}_2 . We discuss the differences in the horizon areas between our solutions and the two-centered Klemm-Sabra solutions which describe the coalescence of two rotating black holes with the spatial topologies of S^3 into a single rotating black hole with the spatial topology of S^3 .

PACS numbers: 04.50.+h, 04.70.Bw

^{*} E-mail: matsuno@sci.osaka-cu.ac.jp

[†] E-mail: ishihara@sci.osaka-cu.ac.jp

[‡] E-mail: mkimura@sci.osaka-cu.ac.jp

[§] E-mail: tomizawa@sci.osaka-cu.ac.jp

I. INTRODUCTION

Since the advent of the TeV gravity scenarios, i.e., the ADD model [1] and the brane world scenario [2, 3], higher dimensional black objects have been attracting renewed interest. One of the reasons is that higher dimensional rotating mini-black holes would be produced by the collision of protons in the Large Hadron Collider (LHC) in these scenarios. It would be possible that one detect the Hawking radiation from these black holes [4, 5, 6, 7, 8]. Once such black hole productions occur, we could expect some of formed rotating black holes to coalesce. These physical phenomena are expected to give us new informations on the extra dimensions. Hence, the discovery of new higher dimensional black hole solutions would play a crucial role in opening a window to extra dimensions.

Higher dimensional black hole solutions has more interesting properties than the four-dimensional one. For instance, in the five-dimensional Einstein theory, there are two types of stationary rotating black hole solutions with the different horizon topologies, that is, S^3 [9] and $S^2 \times S^1$ horizon [10, 11, 12]. Both of the solutions asymptote to the five-dimensional Minkowski spacetime at infinity. Furthermore, a lot of asymptotically flat supersymmetric black object solutions have been found by various authors. The BMPV (Breckenridge, Myers, Peet and Vafa) black hole solutions [13] and the supersymmetric black ring solutions were also found [14] in the five-dimensional $N = 2$ supergravity theory which is one of effective theories of the superstring theory and contains the five-dimensional Maxwell field with a Chern-Simons term [15].

Most authors have considered mainly asymptotically flat and stationary higher dimensional black hole solutions since they would be idealized models if such black holes are small enough for us to neglect the tension of a brane or effects of compactness of extra dimensions. However, if not so, we should consider the higher dimensional spacetimes which have another asymptotic structure. Therefore, it is also important to study black hole solutions with a wide class of asymptotic structures. Recently, the black object solutions with non-trivial asymptotic structures have been studied by various authors. For example, Kaluza-Klein black hole solutions with squashed S^3 horizons [16, 17, 18, 19, 20, 21] asymptote to the three-dimensional flat space with a compact twisted S^1 fiber at infinity. The black ring solutions with the same asymptotic structures [22, 23, 24] were found. On the other hand, there exist black object solutions whose spatial infinity has the topological structure of lens spaces $L(n; 1) = S^3/\mathbb{Z}_n$. For instance, the solution [25] represents a pair of non-rotating black holes with S^3/\mathbb{Z}_2 infinity. It was also found that the supersymmetric black ring

solutions with the same asymptotic structure [26].

There are some dynamical black hole solutions in Einstein-Maxwell theory with a positive cosmological constant. In four-dimensional spacetime, Kastor and Traschen found cosmological multi-black hole solutions which describe the coalescence of charged non-rotating black holes by virtue of the positive cosmological constant [27, 28, 29, 30]. London generalized the Kastor-Traschen solutions to higher dimensional ones [31], which describe the coalescence process such that the arbitrary number of non-rotating black holes with spherical topology coalesce into a single non-rotating black hole with spherical topology. Three of the present authors constructed the different type of black hole solutions in the five-dimensional Einstein-Maxwell theory with a positive cosmological constant. As shown in Ref.[32], though both solutions also describe the coalescence processes of black holes by virtue of the existence of the positive cosmological constant, the coalescence processes are essentially different in the following point. In the five-dimensional Kastor-Traschen solutions, two black holes with S^3 horizon coalesce into a single black hole with S^3 horizon, while in the solutions in Ref.[32], two black holes with S^3 horizon coalesce and convert into a single black hole with S^3/\mathbb{Z}_2 horizon on the Eguchi-Hanson space. Such the difference arises from the difference in the asymptotic structure between both solutions.

Klemm and Sabra also generalized the BMPV solutions [13] to the cosmological multi-black hole solutions [33]. The Klemm-Sabra solutions are also regarded as a generalization of the five-dimensional Kastor-Traschen solutions to rotating solutions. As will be shown later, these solutions describe the coalescence of charged rotating multi-black holes with S^3 horizon into a single rotating black hole with S^3 horizon on the flat space. Similarly, we can generalize the non-rotating black hole solutions on Eguchi-Hanson space in Ref.[32] to rotating black hole solutions as the solutions in the five-dimensional Einstein-Maxwell theory with a Chern-Simon term and a positive cosmological constant. This is the aim of this article. We will show that this solutions describe the coalescence of two rotating black holes with S^3 horizon on the Eguchi-Hanson space. We will also clarify how the difference in asymptotic structure between our solutions and the Klemm-Sabra solutions reflects the difference in coalescence of black holes.

Even if the dynamical properties of such solutions are driven by the effect of a cosmological constant, the discoveries of such black hole solutions are important since it is difficult to find exact dynamical black hole solutions in theories without a positive cosmological constant, and no one has ever succeeded in it as far as we know. These black hole solutions are expected that they give us the information of dynamical black holes in asymptotic flat spacetimes in the case of the

sufficiently small cosmological constant.

This article is organized as follows. In Section II, we give the explicit form of the solutions. In Section III, we review the properties of cosmological BMPV solutions found by Klemm and Sabra [33]. In Section IV, we discuss the coalescence processes of two rotating black holes on the Eguchi-Hanson space. We compare the coalescence of black holes in our solutions with that in the two-centered Klemm-Sabra solutions. In particular, we discuss the difference in the horizon area after the coalescence between both solutions. Finally, we give the summary and some discussions.

II. SOLUTIONS

We consider the five-dimensional Einstein-Maxwell system with a positive cosmological constant $\Lambda > 0$ and a Chern-Simons term. The action is given by

$$S = \frac{1}{16\pi G_5} \int d^5x \sqrt{-g} \left[R - F_{\mu\nu} F^{\mu\nu} - 4\Lambda + \frac{2}{3\sqrt{3}} (\sqrt{-g})^{-1} \epsilon^{\mu\nu\rho\sigma\lambda} A_\mu F_{\nu\rho} F_{\sigma\lambda} \right], \quad (1)$$

where R is the five dimensional scalar curvature, $F = dA$ is the 2-form of the five-dimensional gauge field associated with the gauge potential 1-form A and G_5 is the five-dimensional Newton constant. The action (1) with $\Lambda = 0$ is the bosonic part of the ungauged supersymmetric five-dimensional $N = 2$ supergravity theory without vector multiplets [15].

Following this action (1), we can derive the Einstein equation with the positive cosmological constant $\Lambda > 0$

$$R_{\mu\nu} - \frac{1}{2} R g_{\mu\nu} + 2\Lambda g_{\mu\nu} = 2 \left(F_{\mu\lambda} F_{\nu}{}^\lambda - \frac{1}{4} g_{\mu\nu} F_{\rho\sigma} F^{\rho\sigma} \right), \quad (2)$$

and the Maxwell equation

$$F^{\mu\nu}{}_{;\nu} + \frac{1}{2\sqrt{3}} (\sqrt{-g})^{-1} \epsilon^{\mu\nu\rho\sigma\lambda} F_{\nu\rho} F_{\sigma\lambda} = 0. \quad (3)$$

We construct new multi-black hole solutions on the Eguchi-Hanson base space satisfying the equations (2) and (3). The form of the metric and the gauge potential 1-form are

$$ds^2 = -H^{-2} \left[d\tau + \alpha V^{-1} (d\zeta + \omega) \right]^2 + H \left[V^{-1} (dr^2 + r^2 d\Omega_{S^2}^2) + V (d\zeta + \omega)^2 \right], \quad (4)$$

$$A = \frac{\sqrt{3}}{2} H^{-1} \left[d\tau + \alpha V^{-1} (d\zeta + \omega) \right], \quad (5)$$

where H , V^{-1} and ω are given by

$$H = \lambda\tau + \frac{M_1}{|\mathbf{r} - \mathbf{r}_1|} + \frac{M_2}{|\mathbf{r} - \mathbf{r}_2|}, \quad (6)$$

$$V^{-1} = \frac{N}{|\mathbf{r} - \mathbf{r}_1|} + \frac{N}{|\mathbf{r} - \mathbf{r}_2|}, \quad (7)$$

$$\omega = \left[\frac{N(z - z_1)}{|\mathbf{r} - \mathbf{r}_1|} + \frac{N(z - z_2)}{|\mathbf{r} - \mathbf{r}_2|} \right] d\phi, \quad (8)$$

with the constants M_1 , M_2 , N , α and $\lambda = \pm 2\sqrt{\Lambda/3}$. $d\Omega_{S^2}^2 = d\theta^2 + \sin^2\theta d\phi^2$ denotes the metric of the unit two-sphere. The coordinates run the range of $-\infty < \tau < \infty$, $0 \leq r < \infty$, $0 \leq \theta \leq \pi$, $0 \leq \phi \leq 2\pi$ and $0 \leq \zeta \leq 4\pi N$. $\mathbf{r}_i = (x_i, y_i, z_i)$ ($i = 1, 2$) denote position vectors of the i -th nut singularity N on the three-dimensional flat space $d\mathbf{x} \cdot d\mathbf{x}$. The functions H and V^{-1} are the solutions of the Laplace equation on the three-dimensional flat space. The 1-form ω is determined by the equation $\nabla \times \omega = \nabla V^{-1}$.

For the appearance of a constant λ , the solution (4) is dynamical, i.e., it admits no timelike Killing vector field. The parameter α in the metric (4) is an additional parameter for the solution in [32]. If $\alpha = 0$ then the solution (4) describes the coalescence of two non-rotating black holes on the Eguchi-Hanson space [32]. So, we expect that this solution (4) describes the coalescence of extremely charged two black holes with two equal angular momentums on the Eguchi-Hanson space. Here and after, we restrict ourselves to considering the contracting phase with $\lambda = -2\sqrt{\Lambda/3} < 0$ and the range of time $\tau = (-\infty, 0)$.

In this article, we focus on the regions of the neighborhood of $\mathbf{r} = \mathbf{r}_i$ ($i = 1, 2$) and the asymptotic region $r \simeq \infty$ in the solution (4). In the neighborhood of $\mathbf{r} = \mathbf{r}_i$, the above metric (4) approaches to that of the Klemm-Sabra solution [33, 34]. Similarly, in the asymptotic region $r \simeq \infty$, the local geometry of the metric (4) can be regarded as that of the Klemm-Sabra solution. So, in the next section, we review the physical properties of the Klemm-Sabra solution.

III. REVIEW OF KLEMM-SABRA SOLUTION

We review here properties of the Klemm-Sabra solution [33, 34], which is the BMPV black hole [13] with a cosmological constant. The metric in the cosmological coordinates (τ, R) are given by

$$ds^2 = -\left(\lambda\tau + \frac{m}{R^2}\right)^{-2} \left[d\tau + \frac{j}{2R^2} (d\psi + \cos\theta d\phi) \right]^2$$

$$+ \left(\lambda\tau + \frac{m}{R^2} \right) \left[dR^2 + \frac{R^2}{4} \left\{ d\Omega_{S^2}^2 + (d\psi + \cos\theta d\phi)^2 \right\} \right], \quad (9)$$

where m and j are constants which specify the mass and the angular momentum. The curvature singularity exist at $\lambda\tau R^2 = -m$. Indeed, setting τ to be $\tau + \lambda^{-1}$ and taking the limit $\lambda \rightarrow 0$, we find the metric (9) reduces to the BMPV black hole solution [13].

One obtains the expansions θ_{\pm} of the outgoing and ingoing null geodesics for the $\tau = \text{const.}$ and $R = \text{const.}$ surface as

$$\theta_{\pm} = \lambda \pm \frac{2x}{\sqrt{(x+m)^3 - j^2}}, \quad (10)$$

where we introduced a coordinate $x = \lambda\tau R^2$. Thus, the horizon occur at x such that

$$\lambda^2 \left[(x+m)^3 - j^2 \right] - 4x^2 = 0. \quad (11)$$

The solution (9) seems to be dynamical for the dependence of τ , but it is stationary. Actually, one can introduce stationary coordinates $(\hat{t}, \hat{r}, \hat{\psi})$ for the solution (9) as follows,

$$\lambda\tau R^2 = \hat{r}^2 - m, \quad (\lambda\tau)^{-1} d\tau = d\hat{t} + \hat{f}(\hat{r})d\hat{r}, \quad d\psi = d\hat{\psi} + \hat{h}(\hat{r})d\hat{r}, \quad (12)$$

with

$$\hat{f}(\hat{r}) = \frac{2\lambda\hat{r}(\hat{r}^6 - j^2) / (\hat{r}^2 - m)}{\lambda^2(\hat{r}^6 - j^2) - 4(\hat{r}^2 - m)^2}, \quad \hat{h}(\hat{r}) = \frac{4\lambda j\hat{r}}{\lambda^2(\hat{r}^6 - j^2) - 4(\hat{r}^2 - m)^2}. \quad (13)$$

The form of the metric (9) after the above coordinates transformation now becomes

$$ds^2 = \frac{\lambda^2}{4} \hat{r}^2 d\hat{t}^2 - U^2(\hat{r}) \left[d\hat{t} + \frac{j}{2\hat{r}^2} U^{-1}(\hat{r}) (d\hat{\psi} + \cos\theta d\phi) \right]^2 + \frac{d\hat{r}^2}{W(\hat{r})} + \frac{\hat{r}^2}{4} \left[d\Omega_{S^2}^2 + (d\hat{\psi} + \cos\theta d\phi)^2 \right], \quad (14)$$

where the functions $U(\hat{r})$ and $W(\hat{r})$ are

$$U(\hat{r}) = 1 - \frac{m}{\hat{r}^2}, \quad W(\hat{r}) = \left(1 - \frac{m}{\hat{r}^2} \right)^2 - \frac{\lambda^2}{4} \hat{r}^2 + \frac{\lambda^2 j^2}{4\hat{r}^4}. \quad (15)$$

From (11), (12) and (15), we see that the horizon occur at \hat{r} such that $W(\hat{r}) = 0$.

The equation (11) has three real roots x_-, x_+, x_c ($x_- \leq 0 \leq x_+ \leq x_c$), where x_-, x_+, x_c correspond to the inner horizon, the black hole horizon and the cosmological horizon, respectively, if the mass parameter m and the angular momentum parameter j satisfies the following conditions,

$$0 \leq m\lambda^2 \leq \frac{2}{3}, \quad j_-^2(m) \leq j^2 \leq j_+^2(m), \quad (16)$$

where

$$j_{\pm}^2(m) = \frac{4}{27\lambda^6} \left[9m\lambda^2(8 - 3m\lambda^2) - 32 \pm 8\sqrt{2}(2 - 3m\lambda^2)^{3/2} \right]. \quad (17)$$

In the case of $j = j_+$, the black hole horizon x_+ coincides with the inner horizon x_- , and in the case of $j = j_-$, the black hole horizon x_+ coincides with the cosmological horizon x_c . The naked singularity appears if m and j are out of the ranges (16). We draw the region of (m, j) satisfying the condition (16) in FIG.1. Next, we focus on the conditions for the absence of closed timelike curves (CTCs) outside the black hole horizon $x_+(m, j)$. These CTCs occur if and only if the two dimensional (ψ, ϕ) part of the metric (9), namely, g_{2D} has a negative eigenvalue. We must check the condition $g_{\psi\psi} > 0$ and $\det g_{2D} > 0$ for $x > x_+ > 0$. In this case, explicit forms of these components are given by

$$g_{\psi\psi} = \frac{(x+m)^3 - j^2}{4(x+m)^2}, \quad \det g_{2D} = \frac{(x+m)^3 - j^2}{16(x+m)} \sin^2 \theta. \quad (18)$$

Since the numerators of $g_{\psi\psi}$ and $\det g_{2D}$ are monotonically increasing functions of x , it is sufficient to show $g_{\psi\psi} > 0$ and $\det g_{2D} > 0$ on the horizon x_+ . Actually, we see that

$$g_{\psi\psi} = \left[\frac{x_+}{\lambda(x_+ + m)} \right]^2 > 0, \quad \det g_{2D} = \frac{x_+^2}{4\lambda^2(x_+ + m)} \sin^2 \theta > 0, \quad (19)$$

for $x_+ > 0$ and $m > 0$. Fortunately, we obtain the regular black hole solutions with parameters (m, j) satisfying the condition (16) which have no CTCs outside the black hole horizon.

The induced metric on the black hole horizon $x = x_+(m, j)$ becomes

$$ds_H^2 = \frac{x_+ + m}{4} \left[d\Omega_{S^2}^2 + \frac{(x_+ + m)^3 - j^2}{(x_+ + m)^3} (d\psi + \cos \theta d\phi)^2 \right], \quad (20)$$

which implies the shape of horizon is the squashed S^3 , a twisted S^1 fiber bundle over an S^2 base space with the different sizes, for the presence of angular momentum parameter.

From (11) and (20) we obtain the expression of the area of the black hole horizon $x = x_+(m, j)$ as

$$A_H = \frac{2}{\lambda} x_+(m, j) A_{S^3}, \quad (21)$$

where A_{S^3} denotes the area of the unit S^3 . We will see the change in the horizon area before and after coalescence with this expression (21).

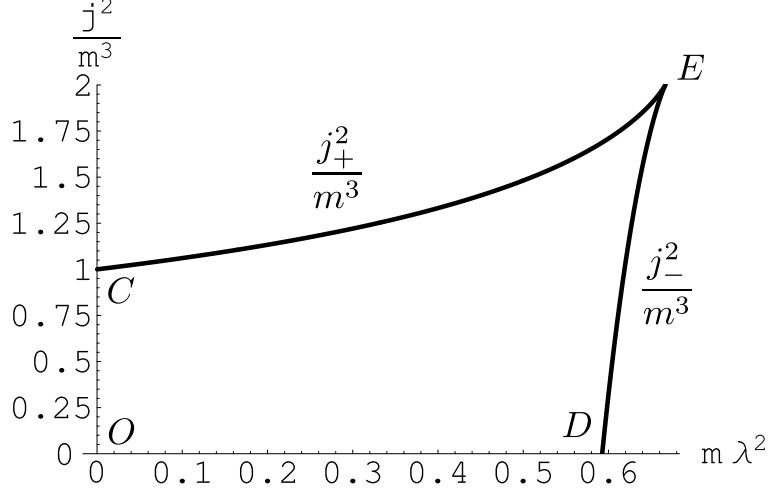


FIG. 1: This figure shows the region of parameters such that the solutions have no naked singularity. The vertical axis and the horizontal axis denote j^2/m^3 and $m\lambda^2$, respectively. The curves CE and DE correspond to $j^2/m^3 = j_+^2/m^3$ and $j^2/m^3 = j_-^2/m^3$, respectively. The solutions lying in the region $ODEC$ have three horizons. On CE the black hole horizon x_+ coincides with the inner horizon x_- and on DE the black hole horizon x_+ coincides with the cosmological horizon x_c . Outside the region $ODEC$ there exist naked singularities.

IV. COALESCENCE OF TWO ROTATING BLACK HOLES

A. Asymptotic Behavior of Black Holes at Early Time and Late Time

First, we investigate the asymptotic behaviors of the metric (4) in the neighborhood of $\mathbf{r} = \mathbf{r}_i$ ($i = 1, 2$). In this region, the metric (4) takes the form of

$$ds^2 \simeq -\left(\lambda\tau + \frac{m_i}{\tilde{r}^2}\right)^{-2} \left[d\tau + \frac{j}{2\tilde{r}^2} (d\psi + \cos\theta d\phi) \right]^2 + \left(\lambda\tau + \frac{m_i}{\tilde{r}^2}\right) \left[d\tilde{r}^2 + \frac{\tilde{r}^2}{4} \left\{ d\Omega_{S^2}^2 + (d\psi + \cos\theta d\phi)^2 \right\} \right], \quad (22)$$

where we introduced the coordinates $\tilde{r}^2 = 4Nr$, $\psi = \zeta/N$, $m_i = 4NM_i$ and $j = 8\alpha N^3$. This metric is equal to that of the Klemm-Sabra solutions (9) with the mass parameters m_i and the angular momentum parameter j . As discussed in the previous section III, this solution (22) admits three horizons at $x = x_{\pm}$, x_c , in the coordinate $x = \lambda\tau\tilde{r}^2$. At the early time $\tau \simeq -\infty$, sufficiently small squashed S^3 spheres centered at $\mathbf{r} = \mathbf{r}_i$ are always outer trapped since there are solutions for $\theta_{\pm} = 0$ at $\tilde{r}^2 = x_{\pm}(m_i, j)/(\lambda\tau)$. Thus, at the early time, there are two rotating black holes with the horizon

topology S^3 .

Next, we focus on the asymptotic region of the solution (4), $r \simeq \infty$. We assume the separation of two black holes $|\mathbf{r}_1 - \mathbf{r}_2|$ is much smaller than r . In this region, the metric (4) behaves as

$$ds^2 \simeq - \left[\lambda\tau + \frac{2(m_1 + m_2)}{\rho^2} \right]^{-2} \left[d\tau + \frac{8j}{2\rho^2} \left(\frac{d\psi}{2} + \cos\theta d\phi \right) \right]^2 + \left[\lambda\tau + \frac{2(m_1 + m_2)}{\rho^2} \right] \left[d\rho^2 + \frac{\rho^2}{4} \left\{ d\Omega_{S^2}^2 + \left(\frac{d\psi}{2} + \cos\theta d\phi \right)^2 \right\} \right], \quad (23)$$

where we introduced the coordinates $\rho^2 = 8Nr$, $\psi = \zeta/N$ and parameters $m_i = 4NM_i$ and $j = 8\alpha N^3$, as same as in (22). This metric (23) resembles that of the Klemm-Sabra solution (9) with the mass parameter $2(m_1 + m_2)$ and angular momentum parameter $8j$.

Like the Klemm-Sabra solution (9), at the late time $\tau \simeq 0$, sufficiently large squashed S^3 sphere becomes outer trapped, since $\theta_+ = 0$ at $\rho^2 = x_+(2(m_1 + m_2), 8j)/(\lambda\tau)$, which give an approximately large sphere. However, we see this solution (23) differs from the Klemm-Sabra solution (9) in the following point; each $\rho = \text{const.}$ surface in the $\tau = \text{const.}$ hypersurface of the metric (23) denotes topologically the lens space S^3/\mathbb{Z}_2 , while in the Klemm-Sabra solution (9), it is diffeomorphic to S^3 . The difference between these metrics appears in (22) and (23): a term $d\psi$ in S^3 metric (22) is replaced by a term $d\psi/2$ in S^3/\mathbb{Z}_2 metric (23). Therefore, at the late time $\tau \simeq 0$, the topology of the outer trapped surface is the lens space S^3/\mathbb{Z}_2 .

Hence, from these results, we find that the solution (4) describes the dynamical situation such that two rotating black holes with the spatial topologies of S^3 coalesce and convert into a single rotating black hole with the spatial topology of the lens space S^3/\mathbb{Z}_2 . Thus, at the early time, there are two rotating black holes specified by (m_1, j) and (m_2, j) . At the late time, there is a single rotating black hole specified by $(2(m_1 + m_2), j)$. Here and after, we call such relations ‘‘mapping rule’’.

B. Typical Processes in Klemm-Sabra solutions

We compare the coalescence processes described by our solutions (4) with the coalescence of two rotating black holes with S^3 horizon into a single rotating black hole with S^3 horizon. For this purpose, let us extend a single Klemm-Sabra solution (9) to the two-centered Klemm-Sabra solution which denotes two rotating black holes with mass parameters m_1, m_2 and angular

momentum parameters j_1, j_2 at the early time,

$$ds^2 = -H^{-2} \left(d\tau + dx^a J_a^b \partial_b K \right)^2 + H dx \cdot dx, \quad (24)$$

with

$$H = \lambda\tau + \frac{m_1}{|\mathbf{x} - \mathbf{x}_1|^2} + \frac{m_2}{|\mathbf{x} - \mathbf{x}_2|^2}, \quad (25)$$

$$K = \frac{j_1/2}{|\mathbf{x} - \mathbf{x}_1|^2} + \frac{j_2/2}{|\mathbf{x} - \mathbf{x}_2|^2}, \quad (26)$$

where J is a complex structure, $\mathbf{x} = (x, y, z, w)$, \mathbf{x}_i ($i = 1, 2$) are position vectors in \mathbb{E}^4 and m_i, j_i are positive constants. The ‘‘mapping rule’’ for this solution (24) becomes as follows; At the early time, there are two rotating black holes specified by (m_1, j_1) and (m_2, j_2) . At the late time, there is a single rotating black hole specified by $(m_1 + m_2, j_1 + j_2)$.

Here, to compare our solution (4) with this solution (24), we restrict ourselves to the solution (24) with the same mass parameters $m = m_1 = m_2$ and the same angular momentum parameters $j = j_1 = j_2$. According to this ‘‘mapping rule’’, we discuss types of process by using dimensionless parameters $m\lambda^2$ and j^2/m^3 . These parameters are mapped as $(m\lambda^2, j^2/m^3) \rightarrow (2m\lambda^2, (j^2/m^3)/2)$ (see FIG.2).

Any solutions lying in the region *ODEC* describe regular initial condition such that there exist two isolated apparent horizons. In contrast, according to the above ‘‘mapping rule’’, any solutions lying in the region *OGKL* describe a single rotating black hole with S^3 horizon at the late time. So, any solutions lying in the region *OGHC* describe a coalescence of two rotating black holes. There are four types of regions, namely, *OGHC*, *GDEH*, *CHKL* and outside of *DEHKL*. These regions correspond to the four kinds of process. The blue dashed arrows represent typical processes.

The process $a \rightarrow a'$ describes the situation such that two rotating black holes with S^3 horizon coalesce and convert into a single rotating black hole with S^3 horizon. The arrow $b \rightarrow b'$ describes the situation such that there are two isolated apparent horizons at the early time, and there exist a naked singularity at the late time. The process $c \rightarrow c'$ describes the situation such that there is not an apparent horizon and CTCs appear at the early time, and at the late time, there exist a single rotating black hole with S^3 horizon and there is no CTC outside the horizon.

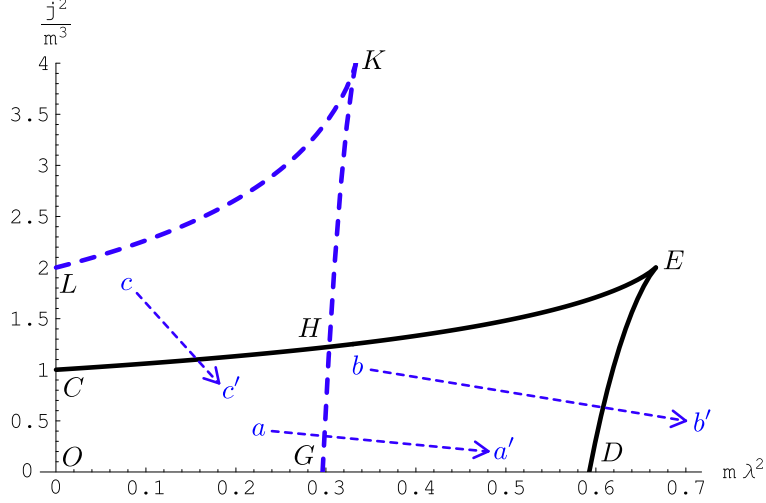


FIG. 2: This figure shows typical processes described by the two-centered Klemm-Sabra solutions (24).

C. Typical Processes in our solutions

Our solutions (4) also describe similar processes to those described by two center Klemm-Sabra solution (24). Now, we compare our cases with two-centered Klemm-Sabra's cases. We restrict ourselves to the solution (4) with the same mass parameters $m = m_1 = m_2$. According to the “mapping rule” of our solutions (4), the dimensionless parameters $m\lambda^2$ and j^2/m^3 are mapped as $(m\lambda^2, j^2/m^3) \rightarrow (4m\lambda^2, j^2/m^3)$ (see FIG.3).

As shown in FIG.2, any solutions lying in the region $ODEC$ describe regular initial condition such that there exist two isolated apparent horizons. In contrast, according to the “mapping rule” of our solution (4), any solutions lying in the region $O AFC$ describe a single rotating black hole with S^3/\mathbb{Z}_2 horizon at the late time. So, any solutions lying in the region $OABC$ describe a coalescence of two rotating black holes. There are four types of regions, namely, $OABC$, $ADEB$, CBF and outside of $DEBFC$. These regions correspond to the four kinds of process. The red dashed arrows represent typical processes.

The process $d \rightarrow d'$ describes the situation such that two rotating black holes with S^3 horizon coalesce and convert into a single rotating black hole with S^3/\mathbb{Z}_2 horizon. The arrow $e \rightarrow e'$ describes the situation such that there are two isolated apparent horizons at the early time, and there exist a naked singularity at the late time. The process $f \rightarrow f'$ describes the situation such that there is not an apparent horizon but CTCs at the early time, while at the late time, there exist a single rotating black hole with S^3/\mathbb{Z}_2 horizon and there is no CTC outside the horizon.

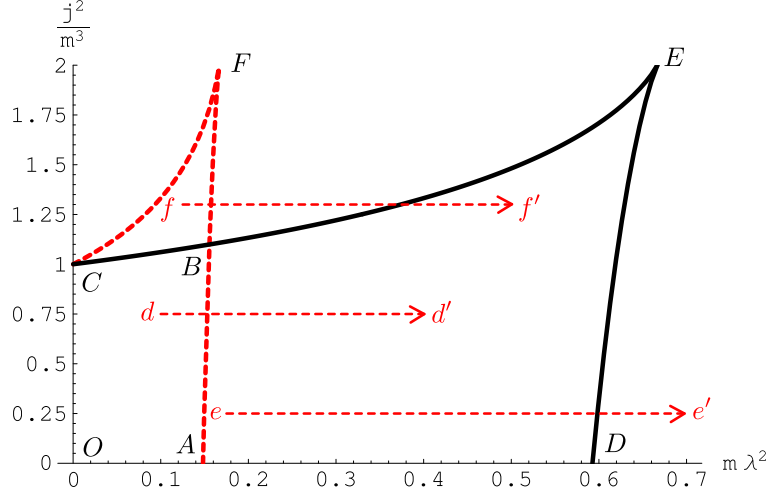


FIG. 3: This figure shows typical processes described by our solutions (4).

From above discussions, there is the featuring difference in “mapping rule” between our solution (4) and two-centered Klemm-Sabra solution (24) in the region $BHKLCF$ in FIG.4. At the early time, both solutions in this region have no apparent horizon. At the late time, the two-centered Klemm-Sabra solution (24) describes a single rotating black hole with S^3 horizon while our solution (4) describes a naked singularity.

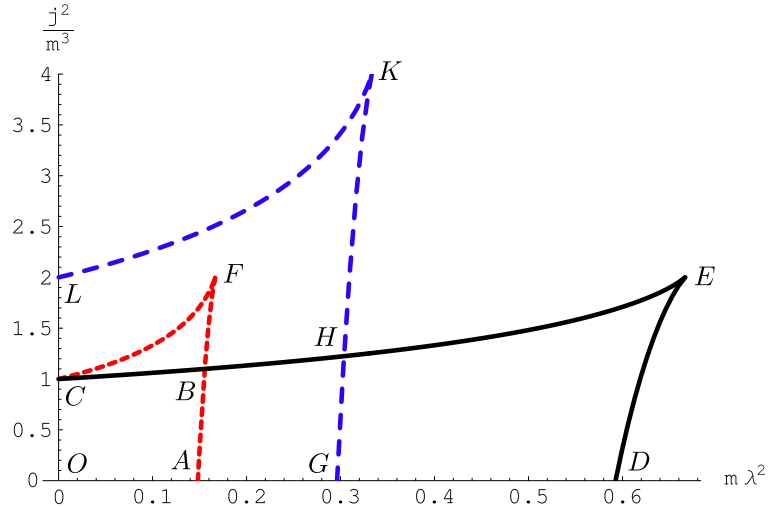


FIG. 4: This figure shows the superposition of FIG.2 and FIG.3.

D. Comparison of Horizon Areas

We compare the area of a single rotating black hole formed by the coalescence of two rotating black holes at the late time. We assume that each black hole in our solution (4) has the same mass, angular momentum and horizon area as that in the two-centered Klemm-Sabra solution at the early time. Then, from the equation (21), the horizon areas in Klemm-Sabra solutions and our solutions at the early time, $A_{\text{Flat}}^{(e)}$ and $A_{\text{EH}}^{(e)}$, are given by

$$A_{\text{Flat}}^{(e)} = A_{\text{EH}}^{(e)} = 2 \times \frac{2}{\lambda} x_+(m, j) A_{\text{S}^3}. \quad (27)$$

On the other hand, according to the ‘‘mapping rules’’ of both solutions, the horizon areas at the late time, $A_{\text{Flat}}^{(l)}$ and $A_{\text{EH}}^{(l)}$, are given by

$$A_{\text{Flat}}^{(l)} = \frac{2}{\lambda} x_+(2m, 2j) A_{\text{S}^3}, \quad (28)$$

$$A_{\text{EH}}^{(l)} = \frac{2}{\lambda} x_+(4m, 8j) \frac{A_{\text{S}^3}}{2}, \quad (29)$$

respectively. Note the factor 1/2 in the equation (29) reflects the fact that the black hole at the late time after coalescence of two black holes is topologically the lens space S^3/\mathbb{Z}_2 .

Now, we consider the ratio of horizon areas at the early time to at the late time $A^{(l)}/A^{(e)}$ in both solutions. The dependence of the ratio on $(m\lambda^2, j^2/m^3)$ in Klemm-Sabra solution is shown in FIG.5. The same in our solution is shown in FIG.6. In all regions, $A_{\text{Flat}}^{(l)}/A_{\text{Flat}}^{(e)} > 1$ and $A_{\text{EH}}^{(l)}/A_{\text{EH}}^{(e)} > 1$. This means that the horizon areas increase by the coalescence. Qualitative behavior of the ratio near the boundary GH in FIG.5 is similar to that near the boundary AB in FIG.6.

However, the behaviors of the ratio near OC are different. Here, we focus on the behaviors in $\lambda \rightarrow 0$ limit. From FIG.5, the ratio $A_{\text{Flat}}^{(l)}/A_{\text{Flat}}^{(e)}|_{\lambda \rightarrow 0} = \sqrt{(2m^3 - j^2)/(m^3 - j^2)}$ depends on the ratio j^2/m^3 along the line OC . In contrast, from FIG.6, the ratio of horizon is independent of the ratio j^2/m^3 , that is, $A_{\text{EH}}^{(l)}/A_{\text{EH}}^{(e)}|_{\lambda \rightarrow 0} = 2$ on the line OC .

In turn, to clarify the differences in the ratio of the horizon areas of two-centered Klemm-Sabra solution to that of our solution, we consider the ratio $A_{\text{EH}}^{(l)}/A_{\text{Flat}}^{(l)}$. FIG.7 shows the dependence of $A_{\text{EH}}^{(l)}/A_{\text{Flat}}^{(l)}$ on $(m\lambda^2, j^2/m^3)$. FIG.8 and FIG.9 show the behaviors of $A_{\text{EH}}^{(l)}/A_{\text{Flat}}^{(l)}$ along the two boundaries, line OA and line OC , respectively. FIG.8 corresponds to the $j = 0$ case which was discussed in [32]. In the non-rotating case, the ratio always satisfies $\sqrt{2} < A_{\text{EH}}^{(l)}/A_{\text{Flat}}^{(l)} < 4$. However in rotating case there is a situation such that $0 < A_{\text{EH}}^{(l)}/A_{\text{Flat}}^{(l)} < \sqrt{2}$ in the region OSC in FIG.7.

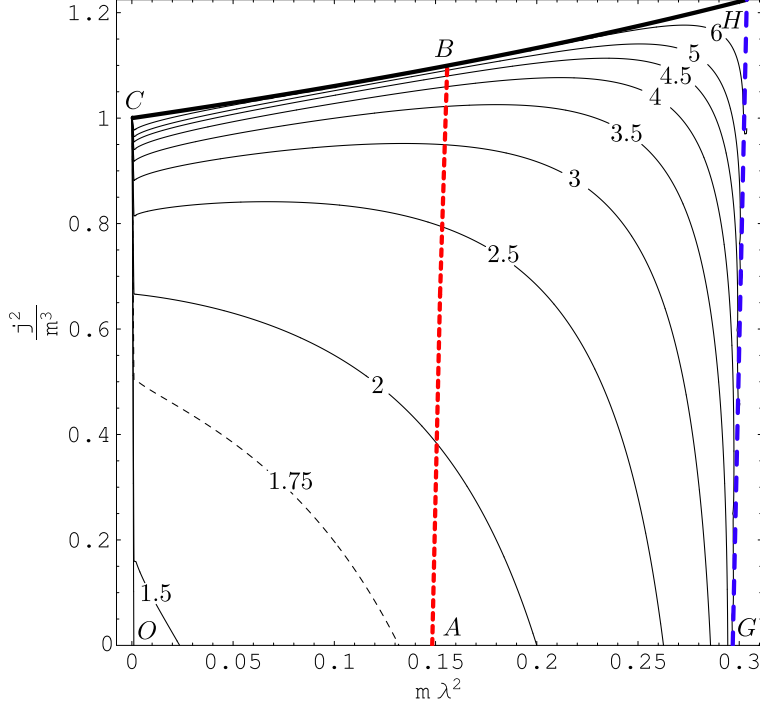


FIG. 5: This figure shows the dependence of the ratio $A_{\text{Flat}}^{(l)}/A_{\text{Flat}}^{(e)}$ on $m\lambda^2$ (horizontal axis) and j^2/m^3 (vertical axis). The curves in this figure denote $A_{\text{Flat}}^{(l)}/A_{\text{Flat}}^{(e)} = \text{const.}$

V. SUMMARY AND DISCUSSION

We have constructed new charged rotating multi-black hole solutions on the Eguchi-Hanson space in the five-dimensional Einstein-Maxwell system with a Chern-Simons term and a positive cosmological constant. These solutions have the mass parameter m_i for each black hole and the common angular momentum parameter. In the case of two black holes with $m_1 = m_2 = m$ for simplicity, by virtue of the positive cosmological constant, these solutions within some region of the parameters (m, j) describe the situation such that two rotating black holes with S^3 horizon coalesce and convert into a single rotating black hole with the S^3/\mathbb{Z}_2 horizon. On the other hand, two-centered Klemm-Sabra solutions describe the physical situation such that two rotating black holes with S^3 horizon coalesce into a single rotating black hole with S^3 horizon.

We have also discussed the difference in the horizon area between our solutions and the two-centered Klemm-Sabra solutions. We have set the same initial condition in both solutions as follows: two black holes have the same masses and angular momentum. In non-rotating case, the ratio of areas of black hole after coalescence is $\sqrt{2} < A_{\text{EH}}^{(l)}/A_{\text{Flat}}^{(l)} < 4$ [32]. In contrast, for the large

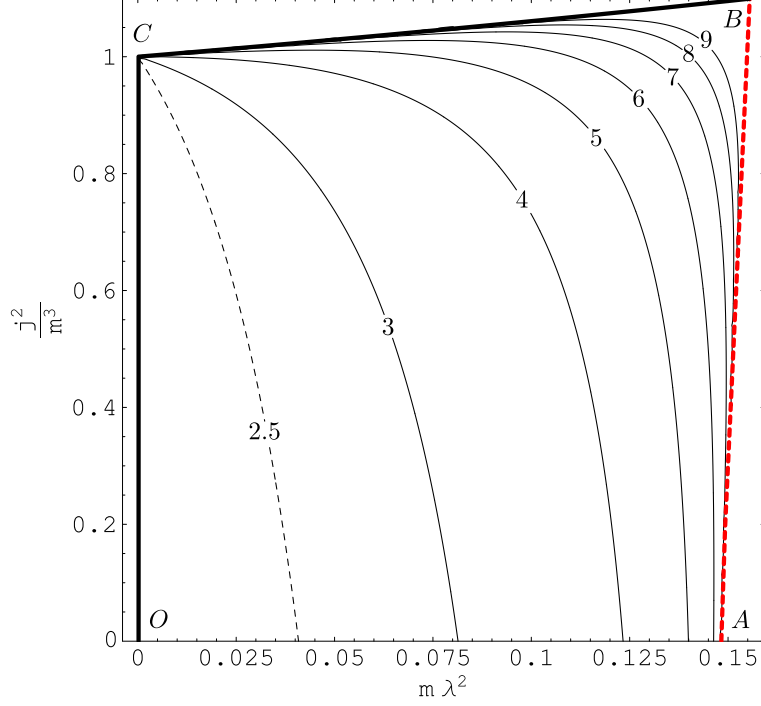


FIG. 6: This figure shows the dependence of the ratio $A_{\text{EH}}^{(l)}/A_{\text{EH}}^{(e)}$ on $m\lambda^2$ (horizontal axis) and j^2/m^3 (vertical axis). The curves in this figure denote $A_{\text{EH}}^{(l)}/A_{\text{EH}}^{(e)} = \text{const.}$

angular momentum in the rotating case, there is the region of parameters where the ratio of the horizon areas becomes $0 < A_{\text{EH}}^{(l)}/A_{\text{Flat}}^{(l)} < \sqrt{2}$.

As mentioned in Introduction, both solutions in this article describe the coalescence of black holes by virtue of a positive cosmological constant. Nevertheless, in $\lambda \rightarrow 0$ limit our results would suggest some information about the coalescence of two rotating supersymmetric black holes on the flat space (BMPV solutions) and on the Eguchi-Hanson space. Therefore, let us discuss the limit $\lambda \rightarrow 0$. Two rotating supersymmetric black holes characterized by the parameters (m, j) with a total horizon area $A^{(e)}$ coalesce into a single rotating supersymmetric black hole with a horizon area $A_{\text{Flat}}^{(l)} = \sqrt{(2m^3 - j^2)/(m^3 - j^2)}A_{\text{Flat}}^{(e)}$ on the flat space, while on the Eguchi-Hanson space $A_{\text{EH}}^{(l)} = 2A_{\text{EH}}^{(e)}$, which is independent of parameters (m, j) . If $2/3 < j^2/m^3 < 1$, the area of black hole horizon after the coalescence on the Eguchi-Hanson space is smaller than that on the flat space, i.e., $0 < A_{\text{EH}}^{(l)}/A_{\text{Flat}}^{(l)} < 1$.

At first sight, the “mapping rule” $(2m, 2j) \rightarrow (4m, 8j)$ for our solutions seems to be inconsistent with the conservation laws of energy and angular momentum. Hence, finally let us check the consistency between the conservation laws and the “mapping rules” in the $\lambda \rightarrow 0$ limit. As

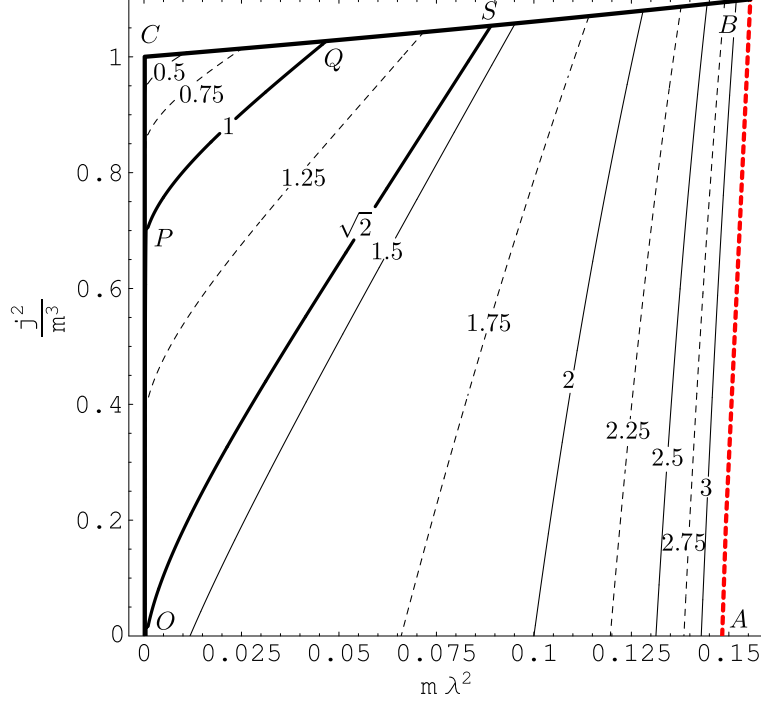


FIG. 7: This figure shows the dependence of the ratio $A_{\text{EH}}^{(l)}/A_{\text{Flat}}^{(l)}$ on $m\lambda^2$ (horizontal axis) and j^2/m^3 (vertical axis). The curves in this figure denote $A_{\text{EH}}^{(l)}/A_{\text{Flat}}^{(l)} = \text{const}$. Here, the ratio of horizon area becomes $0 < A_{\text{EH}}^{(l)}/A_{\text{Flat}}^{(l)} < \sqrt{2}$ in the region OSC . This behavior is one of the unique properties of the solution (4) with a presence of rotations.

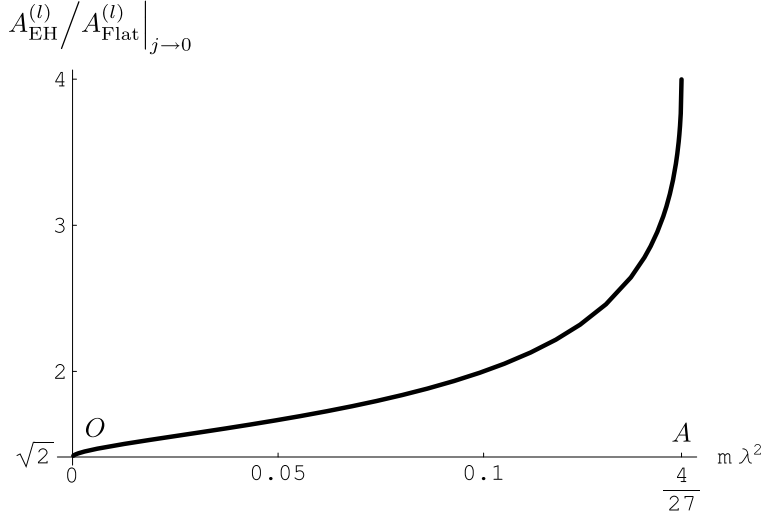


FIG. 8: This figure shows the dependence of $A_{\text{EH}}^{(l)}/A_{\text{Flat}}^{(l)}|_{j \rightarrow 0}$ on $m\lambda^2$ on the line OA . We see that $A_{\text{EH}}^{(l)}/A_{\text{Flat}}^{(l)}|_{j \rightarrow 0}$ is as same as in the non-rotating case [32].

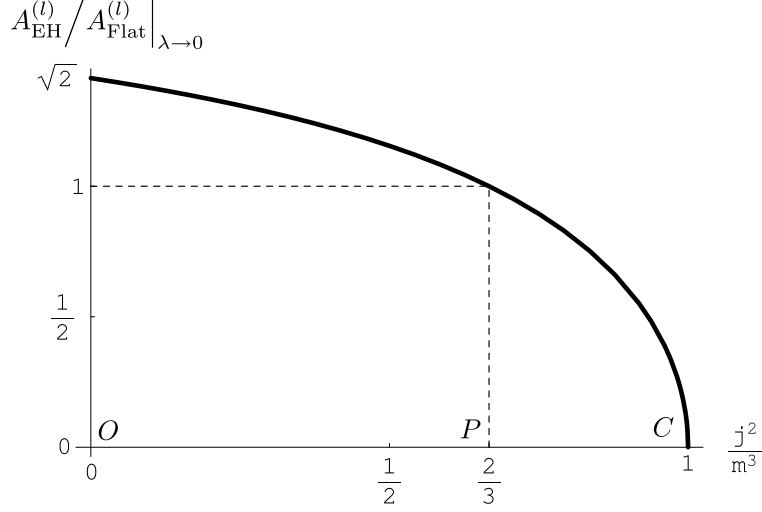


FIG. 9: This figure shows that the dependence of $A_{\text{EH}}^{(l)}/A_{\text{Flat}}^{(l)}|_{\lambda \rightarrow 0}$ on j^2/m^3 on the line OC . For large angular momentum, i.e., $2/3 < j^2/m^3 < 1$, the area of black hole horizon after coalescence on the Eguchi-Hanson space is smaller than that on the flat space, that is, $0 < A_{\text{EH}}^{(l)}/A_{\text{Flat}}^{(l)} < 1$.

discussed in the previous section, we suppose that each black hole on the flat space has the same mass, angular momentum and horizon area as that on the Eguchi-Hanson space at the early time. Then, the total mass and angular momentum at the early time, $M^{(e)}$ and $J^{(e)}$, for two black holes on the flat space and on the Eguchi-Hanson space are given by

$$M_{\text{Flat}}^{(e)} = M_{\text{EH}}^{(e)} = 2 \times \frac{3m}{8\pi G_5} A_{\text{S}^3}, \quad (30)$$

$$J_{\text{Flat}}^{(e)} = J_{\text{EH}}^{(e)} = -2 \times \frac{j}{4\pi G_5} A_{\text{S}^3}, \quad (31)$$

where it is noted that $J_{\text{Flat}}^{(e)}$ and $J_{\text{EH}}^{(e)}$ are the angular momenta associated with the Killing vector field $\partial/\partial\psi$. Of course, these amounts are conserved during the processes, i.e., the total mass and angular momentum at the late time, $M^{(l)}$ and $J^{(l)}$, become $M^{(l)} = M^{(e)}$ and $J^{(l)} = J^{(e)}$. Then $M^{(l)}$ and $J^{(l)}$ for a single black hole on the flat space and on the Eguchi-Hanson space are given by

$$M_{\text{Flat}}^{(l)} = M_{\text{EH}}^{(l)} = \frac{3m}{4\pi G_5} A_{\text{S}^3}, \quad (32)$$

$$J_{\text{Flat}}^{(l)} = J_{\text{EH}}^{(l)} = -\frac{j}{2\pi G_5} A_{\text{S}^3}. \quad (33)$$

On the other hand, according to the “mapping rule” of the two-centered Klemm-Sabra solutions (24) in the $\lambda \rightarrow 0$ limit, the mass and the angular momentum of a single rotating black hole with

the parameters $(2m, 2j)$ after coalescence are given by

$$M_{\text{Flat}}^{(l)} = \frac{3 \times 2m}{8\pi G_5} A_{S^3} = \frac{3m}{4\pi G_5} A_{S^3}, \quad (34)$$

$$J_{\text{Flat}}^{(l)} = -\frac{2j}{4\pi G_5} A_{S^3} = -\frac{j}{2\pi G_5} A_{S^3}. \quad (35)$$

According to the ‘‘mapping rule’’ of our solutions (4) in the $\lambda \rightarrow 0$ limit, while the mass and the angular momentum of a single rotating black hole with the parameters $(4m, 8j)$ after coalescence are given by

$$M_{\text{EH}}^{(l)} = \frac{3 \times 4m}{8\pi G_5} A_{S^3/\mathbb{Z}_2} = \frac{3m}{4\pi G_5} A_{S^3}, \quad (36)$$

$$J_{\text{EH}}^{(l)} = -\frac{8j/2}{4\pi G_5} \frac{A_{S^3}}{2} = -\frac{j}{2\pi G_5} A_{S^3}, \quad (37)$$

where the factor $1/2$ in $8j/2$ of Eq.(37) reflects that the Killing vector we used to compute the angular momentum is $\partial/\partial\psi$ rather than $\partial/\partial(\psi/2)$, and the factor $1/2$ in $A_{S^3}/2$ reflect that the spatial infinity is topologically the lens space S^3/\mathbb{Z}_2 . Then, we see that $M_{\text{Flat}}^{(l)} = M_{\text{EH}}^{(l)}$ from (34), (36) and $J_{\text{Flat}}^{(l)} = J_{\text{EH}}^{(l)}$ from (35), (37). These relations are same as (32) and (33), respectively. Thus, the ‘‘mapping rules’’ of our solutions (4) means only the conservation laws of mass and angular momentum in the $\lambda \rightarrow 0$ case.

Finally, we mention that one can generalize our solution (4) by replacing the harmonics in (6), (7) and (8) by

$$H = \lambda\tau + \sum_i \frac{M_i}{|\mathbf{r} - \mathbf{r}_i|}, \quad V^{-1} = \epsilon + \sum_i \frac{N_i}{|\mathbf{r} - \mathbf{r}_i|}, \quad (38)$$

and

$$\omega = \sum_i \frac{N_i(z - z_i)}{|\mathbf{r} - \mathbf{r}_i|} \frac{(x - x_i)dy - (y - y_i)dx}{(x - x_i)^2 + (y - y_i)^2}, \quad (39)$$

respectively. Here, the constant ϵ takes the value 0 or 1. Black hole solutions on the multi-centered Eguchi-Hanson spaces are obtained by $\epsilon = 0$ with the sum $i \geq 2$. Black hole solutions on the multi-centered-Taub-NUT spaces are obtained by $\epsilon = 1$ with the sum $i \geq 1$. These solutions include some previously known solutions, i.e., cosmological non-rotating multi-black hole solutions on the multi-centered-Taub-NUT space [35] and rotating multi-black hole solutions on the multi-centered-Taub-NUT space with no cosmological constant [36]. We will study the coalescence of rotating multi-black holes on the multi-centered-Taub-NUT space in near future.

Acknowledgments

We would like to thank Yasunari Kurita, Toshiharu Nakagawa, Ken-ichi Nakao and Chul-Moon Yoo for useful discussions. This work is supported by the Grant-in-Aid for Scientific Research No.13135208 and No.19540305.

- [1] N. Arkani-Hamed, S. Dimopoulos and G. Dvali, Phys. Lett. B **429**, 263 (1998).
- [2] L. Randall and R. Sundrum, Phys. Rev. Lett. **83**, 3370 (1999).
- [3] L. Randall and R. Sundrum, Phys. Rev. Lett. **83**, 4690 (1999).
- [4] T. Banks and W. Fischler, hep-th/9906038.
- [5] S.B. Giddings and S. Thomas, Phys. Rev. D **65**, 056010 (2002).
- [6] D. Ida, K. Oda and S.C. Park, Phys. Rev. D **67**, 064025 (2003);
[Erratum-ibid. Phys. Rev. D **69**, 049901 (2004)].
- [7] D. Ida, K. Oda and S.C. Park, Phys. Rev. D **71**, 124039 (2005).
- [8] D. Ida, K. Oda and S.C. Park, Phys. Rev. D **73**, 124022 (2006).
- [9] R.C. Myers and M.J. Perry, Annals Phys. **172**, 304 (1986).
- [10] R. Emparan and H.S. Reall, Phys. Rev. Lett. **88**, 101101 (2002).
- [11] T. Mishima and H. Iguchi, Phys. Rev. D **73**, 044030 (2006).
- [12] A.A. Pomeransky and R.A. Sen'kov, hep-th/0612005.
- [13] J.C. Breckenridge, R.C. Myers, A.W. Peet and C. Vafa, Phys. Lett. B **391**, 93 (1997).
- [14] H. Elvang, R. Emparan, D. Mateos and H.S. Reall, Phys. Rev. Lett. **93**, 211302 (2004).
- [15] M. Gunaydin, G. Sierra and P.K. Townsend, Nucl. Phys. B **253**, 573 (1985).
- [16] P. Dobiasch and D. Maison, Gen. Rel. Grav. **14**, 231 (1982).
- [17] G.W. Gibbons and D.L. Wiltshire, Ann. Phys. **167**, 201 (1986).
- [18] H. Ishihara and K. Matsuno, Prog. Theor. Phys. **116**, 417 (2006).
- [19] T. Wang, Nucl. Phys. B **756**, 86 (2006).
- [20] S.S. Yazadjiev, Phys. Rev. D **74**, 024022 (2006).
- [21] Y. Brihaye and E. Radu, Phys. Lett. B **641**, 212 (2006).
- [22] I. Bena, P. Kraus and N.P. Warner, Phys. Rev. D **72**, 084019 (2005).
- [23] H. Elvang, R. Emparan, D. Mateos and H.S. Reall, JHEP **08**, 042 (2005).

- [24] D. Gaiotto, A. Strominger and X. Yin, JHEP **02**, 023 (2006).
- [25] H. Ishihara, M. Kimura, K. Matsuno and S. Tomizawa, Phys. Rev. D **74**, 047501 (2006).
- [26] S. Tomizawa, H. Ishihara, M. Kimura and K. Matsuno, arXiv:0705.1098 [hep-th].
- [27] D. Kastor and J. Traschen, Phys. Rev. D **47**, 5370 (1993).
- [28] D.R. Brill, G.T. Horowitz, D. Kastor and J. Traschen, Phys. Rev. D **49**, 840 (1994).
- [29] D.R. Brill and S.A. Hayward, Class. Quant. Grav. **11**, 359 (1994).
- [30] K. Nakao, T. Shiromizu and S.A. Hayward, Phys. Rev. D **52**, 796 (1995).
- [31] L.A.J. London, Nucl. Phys. B **434**, 709 (1995).
- [32] H. Ishihara, M. Kimura, S. Tomizawa, Class. Quant. Grav. **23**, L89 (2006).
- [33] D. Klemm and W.A. Sabra, Phys. Lett. B **503**, 147 (2001).
- [34] M.M. Caldarelli, D. Klemm and W.A. Sabra, JHEP **05**, 014 (2001).
- [35] D. Ida, H. Ishihara, M. Kimura, K. Matsuno, Y. Morisawa and S. Tomizawa, Class. Quant. Grav. **24**, 3141 (2007).
- [36] D. Gaiotto, A. Strominger and X. Yin, JHEP **02**, 024 (2006).